Bulletin of the New Zealand Society for Earthquake Engineering, Vol. 57, No. 3, September 2024

RAPID REPAIR OF RC COLUMNS WITH POST-TENSIONED EXTERNAL CLAMPS

Julian D. Rincon[1] and Santiago Pujol[2]

(Submitted *August 2023*; Reviewed *November 2023*; Accepted *May 2024*)

ABSTRACT

A recent technique for repair of damaged reinforced concrete (RC) columns is reviewed. The technique involves the application of external post-tensioned clamps. The clamps are composed of steel angles and high-strength steel rods. The pairs of angles are placed on the corners of the cross-section, and they are connected with steel rods to each other. To evaluate the effectiveness of the repair technique, four large-scale RC columns with insufficient transverse reinforcement were subjected to lateral displacement reversals and constant axial load. The tests were conducted in two phases: initial testing of columns with none to light transverse reinforcement, followed by the application of clamps on the damaged columns and further testing. The study focused on the efficacy of the clamps to a) restore the lateral-carrying capacity of damaged RC columns, and b) increase drift capacity. Variations in lateral expansion of the column core and their plausible correlations with damage and 'repairability' are examined. Within the conditions investigated, two key requirements are proposed for safe column repair: 1) the concrete in damaged columns with cross-sectional expansion exceeding 1% should be replaced or repaired before clamps are applied as a repair measure, and 2) clamps should be proportioned to resist 100% of the maximum plausible shear demand even though perceptible contributions to shear resistance attributable to the concrete were observed in columns repaired before excessive expansion occurred. In columns with crisscrossing inclined cracks leading to lateral cross-sectional expansion of up to 1%, clamps were observed to provide effective shear resistance comparable to what conventional transverse reinforcement can provide.

https://doi.org/10.5459/bnzsee.1653

INTRODUCTION

Past earthquake sequences in California (Landers, 1992), China (Wenchuan, 2008), Japan (Tohoku, 2011), New Zealand (Christchurch, 2010-2011) and Turkey (Van, 2011 & Kahramanmaraş, 2023) have evidenced the importance of quick repair to help recovery, protect people evacuating damaged buildings, and or to reduce further damage caused by aftershocks or additional earthquakes. For example, the 1994 Northridge Earthquake caused the collapse of seven highway bridges in Los Angeles, California, and severe damage of many others, resulting in disruption to post-earthquake evacuation and response [1].

Moment-resisting frames buildings are particularly susceptible to large seismic drift, which can cause severe damage and collapse during earthquakes [2–4]. In these buildings, columns must resist the demands imposed by strong motion and sustain the gravity loads. As the vertical load-carrying capacity of a building is so critical, the repair of RC columns must be undertaken promptly to ensure the structural stability of the entire building.

Over the past few decades, several retrofit and repair techniques have been developed. Techniques such as concrete jacketing [5,6], steel jacketing [7–10], and FRP wrapping [11–13] have been shown to be effective in restoring and improving the deformability and strength of RC columns and bridge piers. Nevertheless, those techniques do not always lend themselves well for rapid repair. Concrete and steel jacketing are labour-intensive and time-consuming techniques, involving casting and curing, and often requiring heavy-lifting equipment during on-site installation. The use of FRP wrapping can present challenges depending on the geographical location and the availability of resources. In some cases, FRP may be prohibitively expensive or even unfeasible because of scarcity of skilled workmanship in the area. In attempts to reduce the cost of FRP, hybrid FRP composite fibres, combining materials like jute or polyester, have been proposed in developing countries such as Algeria [14], Turkey [15], and Thailand [16]. Nonetheless, the application of any type of FRP requires meticulous surface preparation to ensure optimal bonding with the concrete. This process includes through cleaning, removal of loose concrete, crack injection, and surface roughening to enhance the bond strength. Alternatives that are easy to design and implement are needed for rapid repair and retrofit of large inventories of structures after strong ground motion.

Following the Hanshin-Awaji (Kobe) Earthquake on January 17, 1995, the Ministry of Transportation issued a seismic retrofitting notification to railway companies. By 2003, more than 10000 RC columns on the Shinkansen (bullet train) Lines in Japan, which had shear capacity smaller than the shear at flexural capacity, had been retrofitted [17]. Conventional retrofit methods such as steel jacketing was adjusted for rapid implementation by developing mechanical joints that eliminated welding on-site. Nonetheless, many of the RC columns in need of retrofit were located under railway viaducts in spaces often used for stores and offices, especially in urban areas. Hence, it was crucial to develop novel seismic retrofitting techniques suitable for confined areas with limitations on the use of cranes or heavy machinery while ensuring rapid implementation. One of the techniques studied and implemented was the use of external reinforcement with steel bars and steel angles as shown in Figure 1.

[1] *Corresponding Author, PhD Candidate in Earthquake Engineering, University of Canterbury, Christchurch, julian.rincongil@pg.canterbury.ac.nz*
[2] *Professor of Civil Engineering, University of Canterbury, Christchurch, santiago.pujol@canterbury.ac.nz*

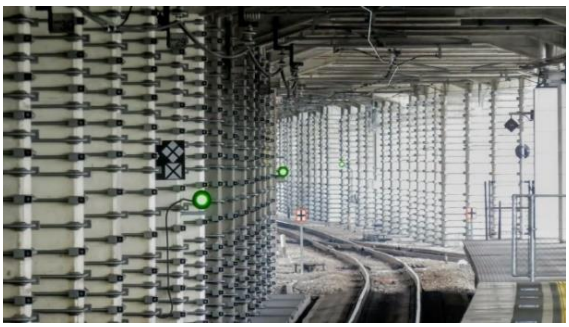

Figure 1: Columns of the Shinkansen railway system with external reinforcement (clamps) [18].

Similar to conventional ties, steel jackets and FRP wraps require formation of cracks and expansion of the concrete core to be engaged, which inevitably relate to perceived damage. This type of confinement can be categorized as 'passive' because it acts in response to cracking and concrete core expansion. Strengthening with passive confinement becomes even less effective in members with existing damage because additional damage is required to engage or activate the added jackets or wraps. In contrast, 'active' confinement, can provide lateral confining pressure before the formation of cracks and expansion of the concrete core. Compared with passive confinement, the use of active confinement in the retrofit and repair of RC columns and bridge piers has received less attention in research. Below, relevant previous research on repair with active confinement is described.

Active confinement involves materials such as shape-memory alloys (SMA), external prestressed strands, steel bars, CFRP or steel straps, among others. In one of the earliest applications of active confinement to retrofit RC members, Lunoe and Willies [19] used external prestressed steel straps in girders of several Air Material Command (AMC) warehouses in 1957.

Yamakawa et al. [20] proposed the use of prestressed aramid belts to retrofit and repair short RC columns. Six columns with shear span to depth ratio of 1.5 and insufficient transverse reinforcement (3.7mm dia. bars @ 105 mm – $r_{tr} = 0.08\%$, Eq. 1) were tested under cyclic loading. External aramid belts were wrapped around the columns and clamped together at the ends by a mechanical coupler. Steel angles protected concrete corners from bearing failure. The technique was evaluated for retrofitting (five columns) and repair (one column). For the test related to repair, the as-built column was initially tested with four prestressed aramid belts with 200 mm spacing to each other. The test continued until a drift ratio of 2.5%, where the lateral carrying capacity dropped more than 20% of the peak shear force. At that point, internal ties had yielded but longitudinal bars had not. The column was then repaired adding six additional prestressed aramid belts. During further testing, these additional belts prevented abrupt shear failure, but the maximum measured lateral force was still smaller than the force associated with flexural yielding.

$$r_{tr} = \frac{A_{tr}}{b \cdot s_{tr}} \quad (1)$$

where:

r_{tr} = transverse reinforcement area ratio of internal ties;
A_{tr} = total area of internal ties within spacing s_{tr};
b = width of the column; and
s_{tr} = spacing of internal ties.

Miyagi et al. [21] proposed the use of steel plates (jacketing), and external prestressed steel bars to repair damaged RC columns with limited transverse reinforcement. The steel plates were placed on the four faces of columns (with square cross-sections), and prestressed steel rods fastened the plates to the column (no welding was necessary). RC columns with cross-sectional dimensions of 250 mm by 250 mm were initially tested to three different damage levels, from cracking (up to 5-mm thick) to damage compromising the axial load carrying capacity of the specimen. This repair technique improved the ductility and lateral and axial load carrying capacity of the specimens. Nonetheless, the repair method was less effective in the specimen with severe damage, in which the lateral-load-carrying capacity could not be increased to reach its flexural strength.

Kyoda et al. [22] focused on economic considerations and ease of installation, proposing the use of polypropylene belts instead of aramid fiber belts, plywood instead of steel plates, and common ratchet buckles instead of bespoke couplers. Experimental results showed the feasibility of the proposed approach for the emergency seismic retrofit of shear-damaged RC columns.

Jung et al. [23] investigated the use of Shape Memory Alloys (SMA) for seismic retrofitting and emergency repair of RC bridge columns with limited displacement capacity. In dynamic earthquake simulations, test columns retrofitted and repaired with SMA were observed to have less damage than reference columns without them. The results showed that SMA confinement was effective in reducing earthquake damage and enhancing the drift capacity of RC columns subjected to strong earthquakes. Nevertheless, SMAs are still relatively expensive, not widely available, and require a training process [24] not suitable for emergency repairs.

In this study, a retrofit technique proposed first by Yamakawa [25] and further tested by Skillen [26] was tested as an alternative for rapid repair of damaged RC columns.

RETROFIT AND REPAIR TECHNIQUE

Yamakawa et al. [25] tested 31 small-scale 250-mm by 250-mm in cross-section RC columns with widely spaced conventional ties. Of the 31 columns, 22 were furnished with external strengthening clamps, the remaining 9 were not. The external clamps consisted of four machined L-shape blocks, bearing against the corners of the column cross-section, and four post-tensioning rods connecting the corner blocks to one another. The columns tested without clamps failed in shear at drift ratios ranging from 0.5% to 1%, while the columns tested with clamps had drift capacities ranging from 1.5% to 5%. Yamakawa defined drift capacity as the maximum drift a column can reach before its lateral load resistance decreases to 80% of the maximum. That drift was determined with the help of an envelope of the load-displacement loops.

More recent work on the use of post-tensioned clamps for retrofit of RC columns was done by Skillen [26], who tested clamps —similar to those used by Yamakawa— in large-scale columns. Skillen's clamps were simpler in that their fabrication did not require machining beyond cutting and drilling (Figure 2). Skillen tested two large-scale RC columns with widely spaced conventional ties. One column was strengthened with post-tensioned clamps, the other column was not. Both columns reached yielding of the longitudinal reinforcement at a drift ratio of approximately 1%. While Column C2 failed in shear at a drift ratio of approximately 1.5%, Column C1 sustained its flexural capacity up to a drift ratio of 7%. Both Yamakawa's and Skillen's test results illustrated the potential of post-tensioned clamps for retrofit of RC columns with insufficient transverse reinforcement. A detailed review of the test results obtained by Yamakawa and Skillen was carried out by the writers in a separate journal article [27].

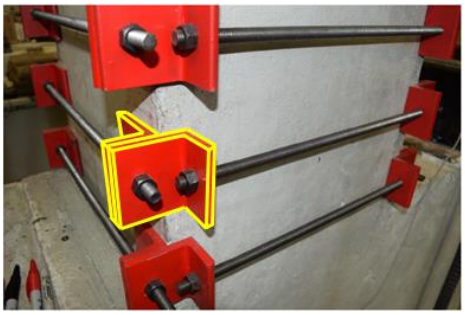

Figure 2: External post-tensioned clamps used by Skillen.

Considering the promising results obtained by Yamakawa and Skillen, a research programme on large-scale columns with post-tensioned clamps as a retrofit measure was launched at the University of Canterbury (UC) in New Zealand followed by additional tests at the National Center for Research on Earthquake Engineering (NCREE) in Taipei, Taiwan. A total of thirteen RC columns furnished with clamps were tested, nine at UC and four at NCREE. The clamps used were similar to those used by Skillen, and the tests were aimed to evaluate the clamps as a retrofit measure. The effects of the posttensioning in the clamps on the column shear strength and drift capacity were discussed in separate journal articles [28,29].

Previous work by Yamakawa, Skillen, and the writers has focused on using the clamps as a retrofit measure. Nonetheless, the simple fabrication and installation process of the clamps may open opportunities for their use as a repair measure. This study explores the effectiveness of the clamps in restoring and increasing the lateral-load capacity and drift capacity of RC columns with initial damage.

EXPERIMENTAL WORK

Specimen Description

Four large-scale RC columns were labelled C10, C11, C12, and C13 (as they were part of the larger experimental programme in retrofit [28,29]). The dimensions and steel reinforcement details are shown in Figure 3. Columns were designed to have high shear stresses and larger dimensions than Yamakawa's columns (250 mm by 250 mm).

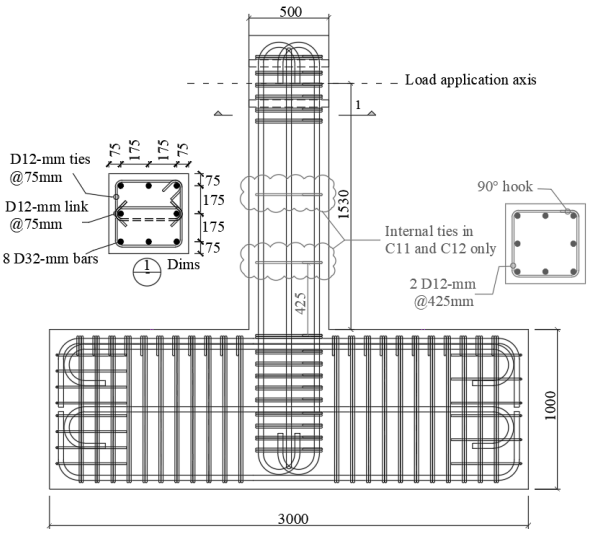

Figure 3: Specimen details.

Columns tested at UC were square in cross-section (500 mm by 500 mm), with a shear span to depth ratio s/d ratio of 3.6, the longitudinal reinforcement consisted of eight bars of 32-mm diameter Gr. 500E AS/NZS 4671 (reinforcement area ratio of 2.6%). Columns C11 and C12 had two ties of 12-mm diameter, spaced at d=425 mm ($r_{tr} = 0.11\%$, Eq. 1), and with 90° hooks, whereas columns C10 and C13 had no internal ties. The low transverse reinforcement ratio in columns tested at UC was chosen to 1) represent a rather extreme case of an older RC column with wide ties spacing, and 2) simplify the estimation of shear resisted by the external transverse reinforcement (clamps).

Each specimen was cast lying on its side, in a single lift, and cured for 7 days under plastic, with water dousing occurring for at least the first 3 days. The concrete mix was supplied by a ready-mix concrete supplier. The cement used was ASTM Type I Portland and the coarse aggregate was a blend of 60% crushed stone (maximum size of 13 mm) and 40% natural alluvial "Greywacke" aggregate (maximum size of 19 mm). The mean cylinder compressive strength measured on the test day of column was 23 MPa. Table 1 summarises the measured material properties. The values reported correspond to the average of results from three coupons. The peak stress corresponds to the maximum measured stress of the stress-strain curve. The uniform strain is the strain associated with the peak stress. The uniform strain is presented instead of the ultimate strain because the former is less sensitive to gauge length, bar size, and the location of the fracture relative to the ends of the gauge.

Table 1: Measured material properties.

	Measured Properties	
Concrete	Cylinder compressive strength at test day [MPa]	23
Longitudinal reinforcement	Yield stress [MPa]	518
	Peak stress [MPa]	647
	Uniform strain [%]	14
12-mm dia. bar (internal ties)	Yield stress [MPa]	550
	Peak stress [MPa]	680
	Uniform strain [%]	13
16-mm dia. rods (threaded rods in clamps)	Yield stress [MPa]	820
	Peak stress [MPa]	922
	Uniform strain [%]	6
14-mm dia. rods (threaded rods in clamps)	Yield stress [MPa]	695
	Peak stress [MPa]	860
	Uniform strain [%]	5

The clamps designed by Skillen (Figure 2) were simpler to fabricate in comparison with the clamps used by Yamakawa. Therefore, that type of clamps was chosen for this research. Figure 4 shows details of the clamps. The corner brackets of the clamps were made with pairs of equal L125x125x16 G300 steel angles. Steel angles were sized so that their flexural strengths - working as cantilevers, i.e., in single curvature- exceeded the strengths of the rods. Concrete bearing stresses associated with rod strengths did not exceed $0.5f'_c$. A key difference between the clamps used by Skillen and those used in this research is that the latter were welded, as illustrated in Figure 4b. Welding was applied to prevent the concentration of shear force in the rods, which can occur when the angle bears against the rod. For emergency applications, nevertheless, welding can be avoided if the clamps are sized assuming their strength is controlled by the rod sections working in shear.

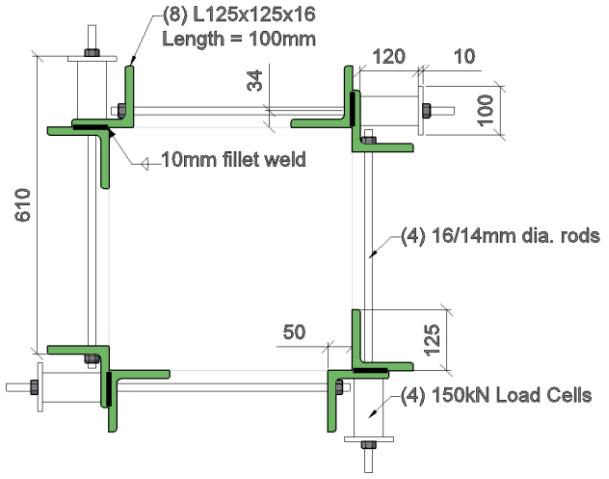

a) Plan View

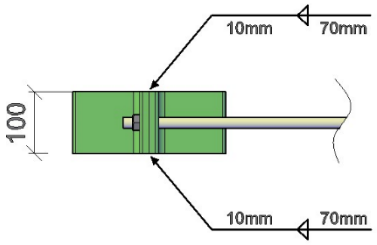

b) Elevation - Welds details

Figure 4: Clamps details.

Except for C13, which had clamps with 14-mm-diamter steel rods, columns had clamps with 16-mm-diameter steel rods. The amount of post-tensioned clamps, calculated using Eq. 2, ranged from 0 to 0.32%.

$$r_{pt} = \frac{A_{pt}}{b \cdot s_{pt}} \quad (2)$$

where:

r_{pt} = transverse reinforcement area ratio of post-tensioned clamps;
A_{pt} = total area of post-tensioned clamps within spacing s_{pt};
b = width of the column; and
s_{pt} = spacing of post-tensioned clamps.

The equivalent lateral confining stress caused by the clamps in the column, σ_L, is expressed as the product of the transverse reinforcement area ratio of clamps and the initial prestress in the clamps, as shown in Eq. 3.

$$\sigma_L = r_{pt} \cdot f_{pti} \quad (3)$$

where:

σ_L= lateral confining stress caused by the clamps in the column;
r_{pt} = transverse reinforcement area ratio of post-tensioned clamps;
f_{pti} = initial prestress in the clamps.

Test columns were designed to be deficient in shear at the start of the test. That is, the nominal unit resistance to shear v_n, calculated using Eq. 4, was smaller than the unit plastic shear stress v_p, calculated using Eq. 5b. As a result, shear failure was expected, and repair was needed. Unit shear stresses are calculated as shear force V divided by the product of the column's width b and effective depth d, $v = V/(bd)$. For simplicity, the effective depth d was taken as the distance from extreme layer of bars in tension to extreme layer of concrete in compression.

$$v_n = v_c + v_s \quad (4)$$

where:

v_n = nominal unit resistance to shear;
v_c = contribution to shear attributed to the concrete; and
v_s = contribution to shear attributed to the transverse reinforcement.

Eq. 4 implies that the total resistance is the sum of contributions assigned to the concrete and the transverse steel reinforcement. Eq. 4 is based on observations made by Richart [30], and was originally derived for conventional ties. Nevertheless, Skillen [26] obtained acceptable results assuming that post-tensioned transverse reinforcement resists shear in a similar fashion to conventional ties. Eq. 4 is rewritten as Eq. 4a for conventional ties and as Eq. 4b for post-tensioned clamps. For columns with both conventional ties and post-tensioned clamps, Eq. 4c was used.

$$v_n = v_c + r_{tr} \cdot f_{try} \quad (4a)$$

$$v_n = v_c + r_{pt} \cdot f_{pty} \quad (4b)$$

$$v_n = v_c + r_{tr} \cdot f_{try} + r_{pt} \cdot f_{pty} \quad (4c)$$

where:

v_n = nominal unit resistance to shear;
v_c = contribution to shear attributed to the concrete;
r_{tr} = transverse reinforcement area ratio of internal ties, calculated using Eq. 1;
f_{try} = yield stress of conventional ties;
r_{pt} = transverse reinforcement area ratio of post-tensioned clamps, calculated using Eq. 2; and
f_{pty} = yield stress of post-tensioned clamps.

The moment capacity M_p at yielding of the longitudinal reinforcement was calculated from a moment-curvature analysis of the column using measured material properties. For the moment-curvature analysis, the following stress-strain relationships were assumed:

- The Hognestad [31] stress-strain relationship for the concrete, with an ultimate strain in the concrete in compression was assumed to be 0.01.
- An elasto-plastic stress-strain relationship for the steel reinforcement.

Equilibrium of the column, working as cantilever over the length h_{clear}, requires the shear force V_p to be:

$$V_p = \frac{M_p}{h_{clear}} \quad (5a)$$

For measured properties (Table 1), V_p is 480 kN and v_p is 2.3 MPa (Eq. 5b).

$$v_p = \frac{V_p}{b \cdot d} \quad (5b)$$

here:

v_p = unit plastic shear stress associated with V_p;
V_p = shear force associated with column bending moment capacity M_p;
b = width of the column;
d = distance from extreme layer of bars in tension to extreme layer of concrete in compression.

Test Setup and Procedure

Figure 5 illustrates the test column and the location of sensors. Columns were tested as single-curvature cantilevers under approximately constant axial load of $0.15A_g f'_c$ and lateral displacement reversals. Axial loads were applied through vertical post-tensioning rods. Lateral displacements were increased in 0.5% drift increments with exception of the first

two increments from 0 to 0.25% and from 0.25 to 0.5%. Three cycles were applied at every target drift ratio. The loading protocol is shown in Figure 6. Testing was paused at points of peak displacement and zero lateral load to record data. Cracks were marked and measured at each peak displacement. Testing concluded when the peak lateral-load in a given cycle was less than 50% of the maximum.

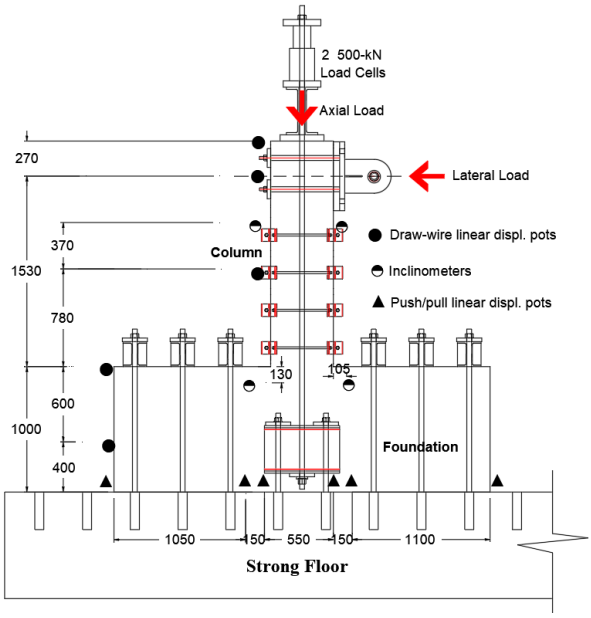

Figure 5: Test setup.

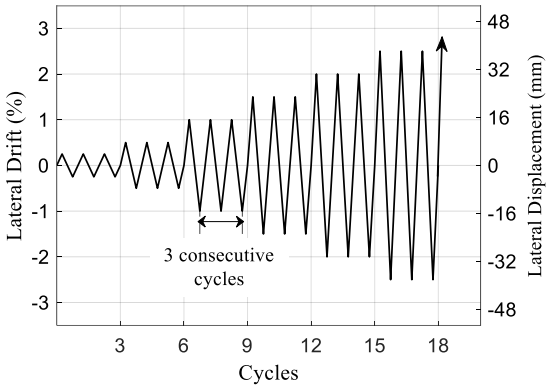

Figure 6: Loading protocol.

The instrumentation used for the tests included:

- Draw-wire linear displacement potentiometers (Model WDS-300-P60-CR-P) with a range of ±150 mm and a resolution of 0.25% of the measuring range.
- Inclinometers (Model NB43210) with a range of ±70 degrees and a resolution of 0.2% of the measuring range.
- Push/pull linear displacement potentiometers (Model S18FLPA30) with a range of ±15 mm and a resolution of 0.7% of the measuring range.

The draw-wire displacement sensors were used to record the displacement of the column at different locations, including the displacement at the axis of application of the lateral load. Inclinometers were used to record any unintended out-of-plane movement and rotations of the foundation. Push/pull displacement sensors were located at both ends of the foundation to record slip displacement, and four others were located on the strong floor at the projection of the column to measure potential uplift.

Additional instrumentation included load cells to record the applied axial and lateral loads to the column, as well as load cells in the clamps. Voltage readings from potentiometers, inclinometers, and load cells were continuously acquired throughout the test duration using an in-house data acquisition system. Concrete core lateral expansion was measured using Particle Tracking Technology (PTT), as described in the next section.

Concrete Core Lateral Expansion (ε_{cc})

Streams V3.03, a software developed by R. Nokes [32–34], was used to estimate the cross-sectional expansion of the concrete core (ε_{cc}) in the columns. Unlike traditional LVDTs and strain gauges that offer only one-directional measurement per device, Streams employs Particle Tracking Technology (PTT) to generate displacement and strain fields.

For the experimental setup (Figure 7***),*** five Fujifilm X-T2 cameras equipped with XF 18–55 lenses were positioned approximately 2 metres from the specimen. Photographs were captured at a resolution of 6000x4000 pixels, while PTT resolution ranged from 0.163 mm/pix to 0.166 mm/pix. Red particles, approximately 4 mm in diameter, were painted onto the concrete surface without following a specific pattern. During tests, an image was captured by each camera at each displacement step of the loading protocol.

Figure 7: Experimental setup for PTT.

To track the particles between image frames, each particle must be matched with particles in the next frame. The collection of positions of a specific particle in every frame comprise the particle path record. In other words, any pair of particles can be treated as a displacement gauge with horizontal and vertical ordinates. A key aspect of this technology is the requirement for traceability of particles in all image frames. The application of PTT on tests where concrete crushing and spalling occur may face challenges due to the loss of particles throughout the test. Therefore, lateral expansion was calculated based on particles that were tracked from the start to the end of each test.

Cross-sectional strains quantifying lateral core expansion, which are discussed in the *Section Analysis of Concrete Core Lateral Expansion*, were calculated using Eq. 6.

$$\varepsilon_{cc_{i-j}} = \frac{L_{i-j} - Lo_{i-j}}{Lo_{i-j}} \quad (6)$$

where:

$\varepsilon_{cc_{i-j}}$ = mean concrete surface strain measured between the ith particle and the jth particle;

L_{i-j} = distance between the i[th] particle and the j[th] particle at the current load step;
Lo_{i-j} = gauge length; distance between the i[th] particle and the j[th] particle at the start of the test.

The gauge length L_o in Eq. 6 ranged from 370 mm to 395 mm ($0.74* b$ to $0.79* b$, with b being the width of the column). The distance from top of foundation (h_g) at which cross-sectional strains were measured ranged from 245 mm to 395 mm ($0.49* h$ to $0.79* h$, with h being the depth of the column). This distance varied from specimen to specimen depending on two considerations:

a) loss of tracked particles caused by spalling, and
b) preference was given to pairs of particles in the section(s) indicating the largest expansion along column height.

Description of Tests Sequence

The experimental programme had the following general objectives:

- Test the clamps on columns with different levels of initial damage: the drift at which the repair was executed ranged from 0.6% to 2.0%.
- Test clamps on columns with different amounts of transverse reinforcement: Columns C10 and C13 did not have internal ties. C13 was furnished with clamps from the start of the test.

Table 2 lists key test variables. The testing of columns C10, C11, and C12 involved two stages: Stages A and B, while column C13 included an additional stage: Stage C. Figure 8 illustrates the drift ratios at which these stages started and finished in each of the tests. Figure 8 also shows sketches indicating which columns had internal ties and when the external clamps were applied. A description of each stage follows.

Table 2: Key test variables.

Spec.	Stage	s_{tr} [mm]	r_{tr} [%]	s_{pt} [mm]	r_{pt} [%]	r_{tot} [%]	σ_L [MPa]
C10	A	-	-	-	-	-	-
	B	-	-	200	0.32	0.32	1.7
C11	A	425	0.11	-	-	0.11	-
	B	425	0.11	425	0.15	0.26	0.8
C12	A	425	0.11	-	-	0.11	-
	B	425	0.11	425	0.15	0.26	0.8
C13	A	-	-	425	0.11	0.11	0.6
	B	-	-	210	0.22	0.22	1.2
	C	-	-	210	0.22	0.22	1.2

where:

s_{tr} = spacing of the internal ties;
r_{tr} = transverse reinforcement area ratio of internal ties, calculated using Eq. 1;
s_{pt} = spacing of the post-tensioned clamps;
r_{pt} = transverse reinforcement area ratio of post-tensioned clamps, calculated using Eq. 2;
r_{tot} = total transverse reinforcement area ratio: sum of area ratio of internal ties and area ratio of post-tensioned clamps;
σ_L = lateral confining stress caused by the clamps in the column, calculated using Eq. 3.

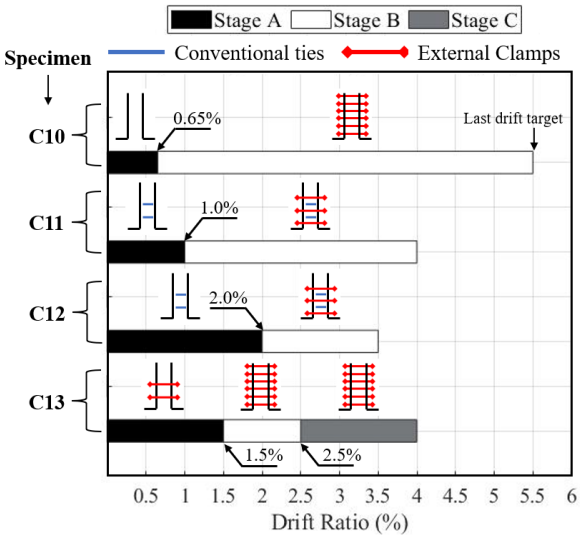

Figure 8: Drift ratios applied in each stage and transverse reinforcement configurations.

Stage A – Initial loading

Stage A induced initial damage ranging from flexural and shear cracking to shear failure. The extent of initial damage depended on the maximum applied drift and the total amount of transverse reinforcement, r_{tot}, defined as the sum of transverse reinforcement area ratios of internal ties and clamps ($r_{tot} = r_{tr} + r_{pt}$). The total amounts of transverse reinforcement r_{tot}, which ranged from 0% for C10 to 0.11% for C13, are listed in Table 2. The maximum applied drift in Stage A is indicated with an arrow in Figure 8.

Stage B – Loading after repair

Stage B corresponded to further loading after repair (described in the Section: *Repair Procedure*). Except for C13, Stage B, was continued until end of test. The test was stopped when the peak load reached during the cycle was smaller than 50% of the maximum load reached in any previous cycle.

Stage C – Further loading in Column C13

Testing of C13 included an additional iteration of repair and loading. Further details regarding the additional repair conducted on C13 and the subsequent loading are provided in the Section: *SPECIFIC OBSERVATIONS*.

Repair Procedure

Following Stage A, columns were repaired by adding post-tensioned clamps. The repair was conducted under zero axial and lateral forces for safety. In the field, shoring of damaged columns would also be required for safety, and it would also reduce the axial load.

With exception of C13, which required grout application, repairs were executed in less than 6 hours and testing was resumed under 24 hours.

The repair procedure can be summarised in the following steps:

1. Placement of temporary supports to facilitate clamps installation, as shown in Figure 9. These supports are useful when a single person executes the installation.
2. Installation of clamps by positioning welded pairs of steel angles (Figure 4) on the four corners of the column and connecting the pairs of angles to each other with steel threaded rods (Figure 10). The clamps were equipped with 150-kN load cells. A machined plate was added to fit the

post-tensioning equipment. Extra length of threaded rod was left on one side for post-tensioning.

Figure 9: Supports made of wood to help installation of steel clamps.

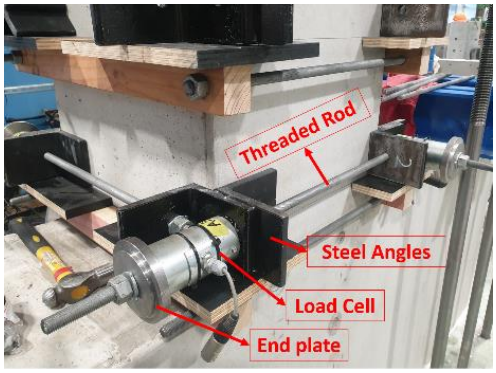

Figure 10: Placing of clamps and load cells.

3. Hand-tightening of the clamps with a spanner to ensure that the steel brackets are firmly in contact with the column corners and are square at all times (Figure 11).

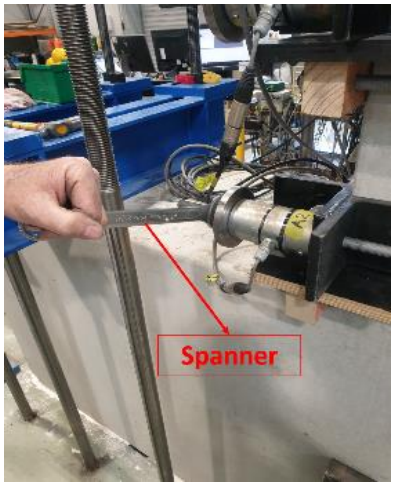

Figure 11: Hand-tightening of clamps.

4. Post-tensioning of the clamps was carried out using an ENERPAC hydraulic bolt tensioner (Model GT-Series) as shown in Figure 12. Gradual increments in force, following a criss-cross tightening sequence, ensured even forces in the rods and prevented rotation of the clamps. In all cases, the clamps were prestressed to approximately 70% of the measured yield stress of the threaded rods.

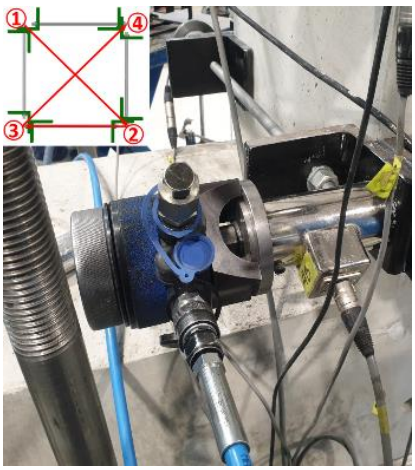

Figure 12: Post-tensioning of clamps.

SPECIFIC OBSERVATIONS

Table **3** presents a detailed summary of test results, including photos of the columns at the end of each loading stage (Figures 13, 15, 16, 18 19, 21, 22, 24, and 25), and load-deflection curves (Figures 14, 17, 20, and 23). Descriptions of test columns and key observations, divided by loading stage, follow Table 3.

Column C10

Stage A

In Stage A, C10 had no transverse reinforcement (conventional ties nor post-tensioned clamps). As a result, its nominal unit resistance to shear v_n (Eq. 4) can be attributed to the resistance to shear of the concrete v_c. At a drift of 0.65%, C10 lost its lateral-load-carrying capacity after the formation of an inclined crack that extended across the entire shear span of the specimen, as shown in Figure 13. This inclined crack occurred at a load of 303 kN, resulting in a shear stress of 1.4 MPa. This shear stress was considered a reasonable estimate of the contribution to shear from the concrete v_c. In all other test columns, a value of $v_c = 1.4$ MPa was used to calculate the nominal unit resistance to shear v_n following Eq. 4. The maximum measured width of the critical shear crack was 4.0 mm. Peak ($\varepsilon_{cc-peak}$) and permanent ($\varepsilon_{cc-perm}$) concrete core lateral expansions, as defined in Table 3 and measured as indicated in the Section: *Concrete Core Lateral Expansion*, were 1.2% and 0.9%, respectively.

Stage B

After Stage A, six post-tensioned clamps were installed on C10, spaced 200 mm apart from each other. The resulting transverse reinforcement area ratio of post-tensioned clamps r_{pt} was 0.32%. The lateral prestress (σ_L=1.7 MPa) reduced the width of the critical shear crack from 4.0 mm to 0.5 mm. The lateral expansion was reduced from 1.2% to 0.1%. The loading protocol was then resumed, starting from the first cycle at a drift ratio of 1%. C10 exhibited flexural yielding at a drift ratio of approximately 1.3%. The maximum measured lateral load V_{max} was 550 kN, which is approximately 15% larger than the shear force associated with flexural capacity V_p, calculated for measured properties (Eq. 5a). The associated shear stress with V_{max} was 2.6 MPa. The existing critical shear crack did not widen, and multiple new flexural and flexure-shear cracks were observed. Figure 15 shows C10 at a drift of -5.5%. The drift capacity, as defined in Table 3, was 5.1%. The lateral expansion at $0.8V_{max}$ was 2.9%, which increased to over 8% at the end of test.

Table 3a: Summary of test results – Column C10.

SPECIMEN C10 - STAGE A		LOAD vs DISPLACEMENT CURVE
C10A	**Internal ties? If yes: (r_{tr} [%])**	No
	**Post-tensioned clamps? If yes: (r_{pt} [%])**	No
	Max. drift ratio [%]:	+0.65*
	V_{max} [kN] (v_{max} in MPa)	+303 (1.4)
	Max. measured flexural crack thickness [mm]:	0.65
	Max. measured shear crack thickness [mm]:	4.0
	Peak concrete core lat. expansion ($\varepsilon_{cc-peak}$) [%]:	1.2
Figure 13: C10 at +0.65% drift - Stage A.	**Permanent concrete core lat. expansion ($\varepsilon_{cc-perm}$) [%]:**	0.9
SPECIMEN C10 - STAGE B		
C10B	**Internal ties? If yes: (r_{tr} [%])**	No
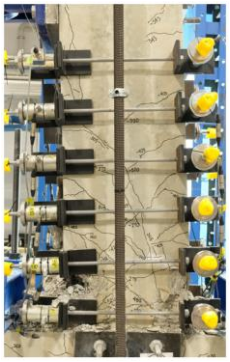	**Post-tensioned clamps? If yes: (r_{pt} [%])**	Yes (0.32)
	Lateral prestress, σ_L [MPa]:	1.7
	ε_{cc} after prestress [%]:	0.1
	$v_s = v_{str} + v_{spt}$ [MPa]:	2.6
	v_s/v_p:	1.1
	Max. drift ratio applied [%]:	±5.5
Figure 15: C10 at -5.5 drift - Stage B.	**V_{max} [kN] (v_{max} in MPa)**	-550 (2.6)

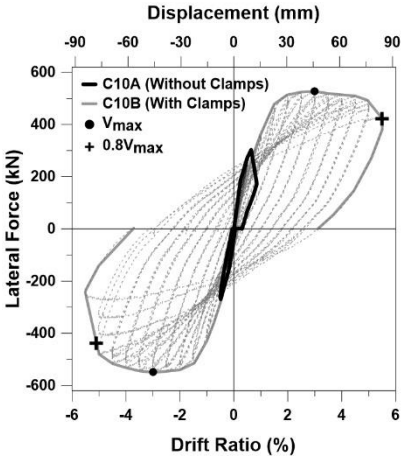

Figure 14: Hysteretic response of C10.

V_{max} [kN] (v_{max} in MPa): -550 (2.6)
v_s/v_{max}: 1.0
D.C.* [%]: 5.1
ε_{cc} at 0.8V_{max} [%]: 2.9
ε_{cc} at end of test [%]: >8

Column C11

Stage A

Column C11 had three conventional ties spaced at 425 mm with the first tie located at $d = 425$ mm from the top face of the foundation. The transverse reinforcement area ratio of internal ties r_{tr} was 0.11%. Inclined shear cracks were observed at a lateral load of 340 kN. The test was stopped after completion of the first cycle at a drift of 1%. The maximum measured shear crack width was 2 mm. The peak concrete core lateral expansion ($\varepsilon_{cc-peak}$) was 0.5%, which did not change after removing the lateral load. Figure 16 shows C11 in the last loading cycle (drift target of 1%) of Stage A.

Stage B

Three post-tensioned clamps were installed on C11, spaced 425 mm apart from each other. The transverse reinforcement area ratio of post-tensioned clamps r_{pt} was 0.15%. The total transverse reinforcement area ratio r_{tot}, calculated as the sum of area ratios of internal ties and post-tensioned clamps, was 0.26%. The total contribution to shear resistance from the transverse reinforcement v_s was equal to 1.8 MPa, calculated as the sum of contributions to shear of the internal ties ($v_{str} = r_{tr} \cdot f_{try}$) and the post-tensioned clamps ($v_{spt} = r_{pt} \cdot f_{pty}$). The lateral prestress (σ_L=0.8 MPa) reduced the concrete lateral expansion from 0.5% to 0.04%. The loading protocol was resumed starting from the second cycle at a drift ratio of 1%. C11 exhibited flexural yielding at a drift ratio of approximately 1.5%. The maximum measured lateral load V_{max} was 525 kN, and the associated shear stress was 2.5 MPa. At a drift ratio of around 3%, flexural-shear cracks developed and extended into the compression zones at the base of the column (Figure 18). The drift capacity was 3.7%. The lateral expansion at 0.8V_{max} was 2.0%, which increased to over 7% at the end of test.

Table 3b: Summary of test results – Column C11.

SPECIMEN C11 (STAGE A)		LOAD vs DISPLACEMENT CURVE
C11A	**Internal ties? If yes: (r_{tr} [%])**	Yes (0.11)
	Post-tensioned clamps? If yes: (r_{pt} [%])	No
	Max. drift ratio [%]:	±1.0*
	Max. lateral force [kN] (stress in MPa)	395 (1.9)
	Max. measured flexural crack thickness [mm]:	1.3
	Max. measured shear crack thickness [mm]:	2
	Peak concrete core lat. expansion ($\varepsilon_{cc-peak}$) [%]:	0.5
	Permanent concrete core lat. expansion ($\varepsilon_{cc-perm}$) [%]:	0.5
SPECIMEN C11 - STAGE B		
C11B	**Internal ties? If yes: (r_{tr} [%])**	Yes (0.11)
	Post-tensioned clamps? If yes: (r_{pt} [%])	Yes (0.15)
	Lateral prestress, σ_L [MPa]:	0.8
	ε_{cc} after prestress [%]:	0.04
	$v_s = v_{str} + v_{spt}$ [MPa]:	2.3
	v_s/v_p:	1.0
	Max. drift ratio applied [%]:	±4.0
	V_{max} [kN] (v_{max} in MPa)	-525 (2.5)

Figure 16: C11 at +1.0 drift - Stage A.

Figure 18: C11 at +4.0 drift - Stage B.

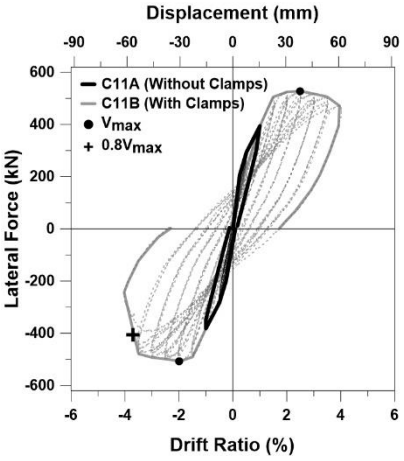

Figure 17: Hysteretic response of C11.

V_{max} [kN] (v_{max} in MPa): 525 (2.5)
v_s/v_{max}: 0.7
D.C. [%]: 3.7
ε_{cc} at 0.8V_{max} [%]: 2
ε_{cc} at end of test [%]: >7

Column C12

Stage A

Column C12, similar to C11, also had three conventional ties spaced at 425 mm (r_{tr}=0.11%). In Stage A, C12 underwent a total of 13 loading cycles, with the final cycle reaching a drift ratio of 2%. The maximum lateral load was 410 kN, which corresponded to a drift ratio of 1.3%. At the final drift ratio of 2%, the lateral load had dropped by 30%, and severe shear disintegration of the concrete was observed (as shown in Figure 19). Comparing the maximum lateral load of 410 kN with the maximum loads measured in the tests of C10 and C11 (550 and 525 kN), it can be concluded that C12 did not develop flexural yielding. The maximum measured shear crack width was 9 mm. The peak concrete core lateral expansion ($\varepsilon_{cc-peak}$) was 5.2%, and the permanent ($\varepsilon_{cc-perm}$) was 4.7%.

Stage B

Column C12 underwent a similar repair process to C11. Three post-tensioned clamps were installed on C12, spaced 425 mm apart from each other (r_{pt}=0.15%). The lateral prestress (σ_L=0.8 MPa) reduced the concrete lateral expansion from 4.7% to 2.5%. The loading protocol was resumed starting from the second cycle at a drift ratio of 2%. The measured shear force at a drift ratio of 2% was 370 kN, which increased to 390 kN at a drift ratio of 2.5%. Nevertheless, the column did not reach flexural yielding, and its lateral-load-carrying capacity decreased rapidly throughout the rest of the test with severe shear disintegration of the concrete core (as shown in Figure 21). The drift capacity was 1.8%, and it was obtained during Stage A of the test. The lateral expansion at 0.8V_{max} was 2.8%, also calculated during Stage A. By the end of the test, the lateral expansion had exceeded 8%.

Column C13

Stage A

At the start of the test, column C13 differed from the other test columns in two aspects:

- C13 was the only column was equipped with clamps in Stage A.

Table 3c: Summary of test results – Column C12.

SPECIMEN C12 (STAGE A)		LOAD vs DISPLACEMENT CURVE
C12A	**Internal ties? If yes: (r_{tr} [%])**	Yes (0.11)
	**Post-tensioned clamps? If yes: (r_{pt} [%])**	No
	Max. drift ratio [%]:	±2.0*
	V_{max} [kN] (v_{max} in MPa)	+410 (1.9)
	Max. measured flexural crack thickness [mm]:	4.0
	Max. measured shear crack thickness [mm]:	9.0
	Peak concrete core lat. expansion ($\varepsilon_{cc-peak}$) [%]:	5.2
Figure 19: C12 at +2.0 drift - Stage A.	**Permanent concrete core lat. expansion ($\varepsilon_{cc-perm}$) [%]:**	4.7
SPECIMEN C12 - STAGE B		
C12B	**Internal ties? If yes: (r_{tr} [%])**	Yes (0.11)
	**Post-tensioned clamps? If yes: (r_{pt} [%])**	Yes (0.15)
	Lateral prestress, σ_L [MPa]:	0.8
	ε_{cc} after prestress [%]:	2.5
	$v_s = v_{str} + v_{spt}$ [MPa]:	1.8
	v_s/v_p:	0.8
	Max. drift ratio applied [%]:	±3.5
Figure 21: C12 at +3.5 drift - Stage B.	**V_{max} [kN] (v_{max} in MPa)**	-400 (1.9)

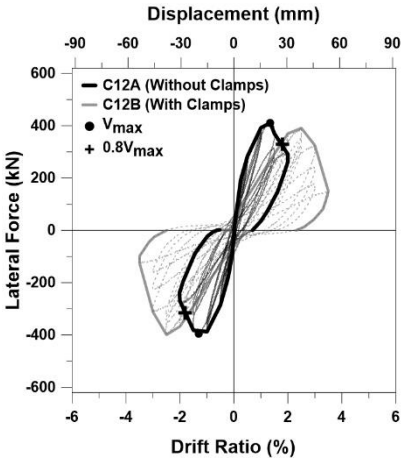

Figure 20: Hysteretic response of C12.

V_{max} [kN] (v_{max} in MPa): 410 (1.9)
v_s/v_{max}: 0.7
D.C. [%]: 1.8
ε_{cc} at 0.8V_{max} [%]: 2.8
ε_{cc} at end of test [%]: >8

- The clamps in C13 were fabricated using 14-mm-diameter steel rods. Other columns had clamps with 16-mm-diameter steel rods. The clamps were located at the same positions (d=425mm and 2*d=850mm) of the first two internal ties in C11 and C12. The purpose of using smaller rods in C13 was to compare columns with the same transverse reinforcement ratio but from different sources. C11 and C12 had conventional ties accounting for r_{tr}=0.11%, while C13 had post-tensioned clamps accounting for r_{pt}=0.11%

The equivalent lateral confining stress σ_L caused by the clamps was 0.6 MPa. The contribution to shear resistance provided by the clamps v_{spt} was 0.8 MPa. In C11 and C12, Stage A was stopped at drift ratios of 1% and 2%, respectively. In contrast, in C13, Stage A concluded with the first cycle at a drift ratio of 1.5%. At this drift ratio, a maximum lateral load of 405 kN was recorded. The maximum measured shear crack width was 2 mm. The peak concrete core lateral expansion ($\varepsilon_{cc-peak}$) was 0.7%, and the permanent ($\varepsilon_{cc-perm}$) was 0.5%.

Stage B

Four additional post-tensioned clamps were installed on column C13. The new clamp spacing was $d/2$ (~215 mm), resulting in a post-tensioned transverse reinforcement ratio r_{pt} equal to 0.22%. The shear resistance provided by the clamps v_{spt} was 1.5 MPa. Applying lateral prestress (σ_L=1.2 MPa) reduced the lateral expansion of the concrete from 0.5% to 0.2%. After repair, the loading protocol was resumed, starting from the second cycle at a drift ratio of 1.5%. At this same drift ratio, C13 exhibited flexural yielding. The maximum measured lateral load V_{max} was 540 kN, and the associated shear stress was 2.5 MPa. During the second cycle at a drift ratio of 2.5%, the second and third clamps (from the base of the column) fractured (Figure 24). Despite the fracture of the clamps, the repair of C13 can be classified as successful in terms of leading to the yielding of the longitudinal reinforcement. As explained in the Section titled "*Analysis of Nominal Shear Resistance vs. Shear Demand*," C13, after repair, had the smallest ratio of resistance to shear provided by the transverse reinforcement to the maximum measured shear stress ($v_s > v_{max} = 0.6$).

The failure in the clamps caused an abrupt decrease in the lateral-load-carrying capacity of C13 as shown in the load-displacement curve in Figure 23. The lateral concrete core expansion increased to 2.1%, and after removing the lateral load, it only reduced to 2%. Stage B was halted, and it was decided to proceed with a second round of repair.

Stage C

In this stage, column C13 underwent a second round of repair and additional loading. The failure in the clamps resulted in the loss of lateral confining pressure on the column and damage to the concrete cover. Reconstruction of the corner areas was necessary before the installation of new clamps (Figure 26). The damaged corners were repaired using SikaGrout 212 HP, a high-strength cementitious grout. After a curing period of two days, the compressive strength of the grout was measured to be 24 MPa, obtained from the average of three 50-mm-side cubes.

After repair, two new clamps were installed and post-tensioned, along with re-tensioning of the existing clamps. The reapplication of lateral prestress (σ_L=1.2 MPa) reduced the lateral expansion of the concrete from 2.1% to 1.5%. The loading protocol was resumed, starting from the third cycle at a drift ratio of 2.5%.

Table 3d: Summary of test results – Column C13.

SPECIMEN C13 - STAGE A		LOAD vs DISPLACEMENT CURVE
C13A	**Internal ties? If yes: (r_{tr} [%])**	No
	Post-tensioned clamps? If yes: (r_{pt} [%])	Yes (0.11)
	Lateral prestress, σ_L [MPa]:	0.6
	Max. drift ratio [%]:	±1.5*
	V_{max} [kN] (v_{max} in MPa)	+475 (2.2)
	Max. measured flexural crack thickness [mm]:	2.1
	Max. measured shear crack thickness [mm]:	2.0
	Peak concrete core lat. expansion ($\varepsilon_{cc-peak}$) [%]:	0.7
	Permanent concrete core lat. expansion ($\varepsilon_{cc-perm}$) [%]:	0.5
SPECIMEN C13 - STAGE B		
C13B	**Internal ties? If yes: (r_{tr} [%])**	No
	Post-tensioned clamps? If yes: (r_{pt} [%])	Yes (0.22)
	Lateral prestress, σ_L [MPa]:	1.2
	ε_{cc} after prestress [%]:	0.2
	$v_s = v_{str} + v_{spt}$ [MPa]:	1.5
	v_s/v_p:	0.6
	Max. drift ratio applied [%]:	±2.5*
	V_{max} [kN] (v_{max} in MPa)	+540 (2.5)
	Max. measured shear crack thickness [mm]:	6
	Peak concrete core lat. expansion ($\varepsilon_{cc-peak}$) [%]:	2.1
	Permanent concrete core lat. expansion ($\varepsilon_{cc-perm}$) [%]:	2

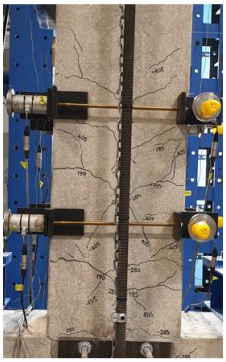

Figure 22: C13 at +1.5 drift - Stage A.

Figure 24: C13 at -2.5 drift - Stage B.

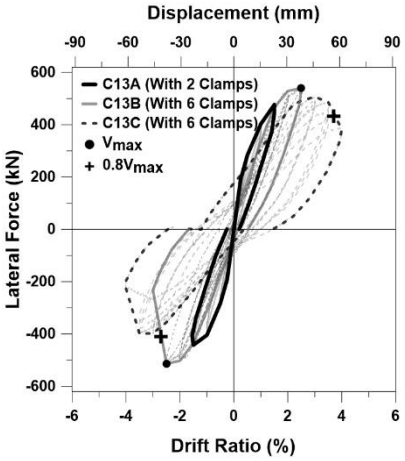

Figure 23: Hysteretic response of C13.

V_{max} [kN] (v_{max} in MPa): 540 (2.5)
v_s/v_{max}: 0.6
D.C. [%]: 2.7
ε_{cc} at 0.8V_{max} [%]: 2.1
ε_{cc} at end of test [%]: >7

SPECIMEN C13 - STAGE C		
C13C	**Internal ties? If yes: (r_{tr} [%])**	No
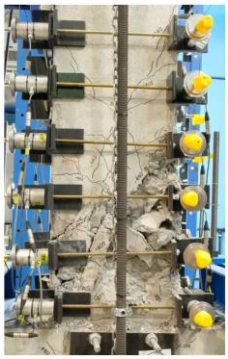	**Post-tensioned clamps? If yes: (r_{pt} [%])**	Yes (0.22)
	Lateral prestress, σ_L [MPa]:	1.2
	ε_{cc} after prestress [%]:	1.5
	$v_s = v_{str} + v_{spt}$ [MPa]:	1.5
	v_s/v_p:	0.6
	Max. drift ratio applied [%]:	±4.0
	V_{max} [kN] (v_{max} in MPa)	+505 (2.4)

Figure 25: C13 at -4.0 drift - Stage C.

Variables in Tables 3a – 3d:

*r_{tr}: transverse reinforcement area ratio of internal ties, calculated using Eq. 1.
*r_{pt}: transverse reinforcement area ratio of post-tensioned clamps, calculated using Eq. 2.
*σ_L: lateral confining stress caused by the clamps in the column, calculated using Eq. 3.
*v_p: unit plastic shear stress associated with V_p, estimated using Eq. 5a.
*V_p: shear force associated with flexural yielding at column base.
*V_{max}: maximum shear force measured in the test.
*v_{max}: shear stress associated with V_{max}, calculated as $V_{max}/(b * d)$.
*v_s: nominal contribution to shear of the transverse reinforcement, including internal ties and external clamps;
*v_{str}: nominal contribution to shear of the conventional ties;
*v_{spt}: nominal contribution to shear of the post-tensioned clamps;
*ε_{cc}: cross-sectional expansion of the concrete core, measured as indicated in the Section: *Concrete Core Lateral Expansion*

***Drift Capacity (D.C)**: drift ratio associated with 20% decrease in the lateral load resistance of the column, and it is calculated with help of an envelope of the load-displacement loops. Two values of drift capacities are obtained (pulling and pushing directions), but only the smaller value is reported.

***Peak Concrete Core Lateral Expansion ($\varepsilon_{cc-peak}$)**: the maximum concrete core expansion measured in the corresponding loading stage. It was measured as indicated in the Section *Concrete Core Lateral Expansion*.

***Permanent Concrete Core Lateral Expansion ($\varepsilon_{cc-perm}$)**: the maximum concrete core expansion measured at the end of the corresponding loading stage, with NO lateral load applied in the column. It was measured as indicated in the Section *Concrete Core Lateral Expansion*.

In Stage C, the maximum measured shear force was 505 kN, which was lower than the previous maximum force of 540 kN measured in Stage B. At a drift ratio of 3%, the lateral-load-carrying capacity decreased by 22% in the pulling direction of the test, which was the loading direction when the clamps failed in Stage B. The drift capacity was 2.7%. The lateral expansion of the concrete at $0.8V_{max}$ was 2.1%. The test was stopped after the first cycle at a drift ratio of 4%, when the lateral-load-carrying capacity had dropped by more than 50%. At the end of the test, the lateral expansion of the concrete core exceeded 7%.

GENERAL OBSERVATIONS

Key test results (e.g. drift capacities and lateral concrete core expansions) and parameters (e.g. v_s/v_{max}) are listed in Tables 4 and 5. Four columns were repaired (C10, C11, C12, and C13). Two repairs worked well (C10B, C11B), one did not (C12B), and one worked but failure was abrupt (C13B). Here, 'successful' repairs are repairs leading to yielding of the longitudinal reinforcement and drift capacities exceeding 2%, or drift capacities exceeding what would be expected for a column with conventional ties as illustrated in Figure 27.

Figure 26: Repair of C13 – Stage C.

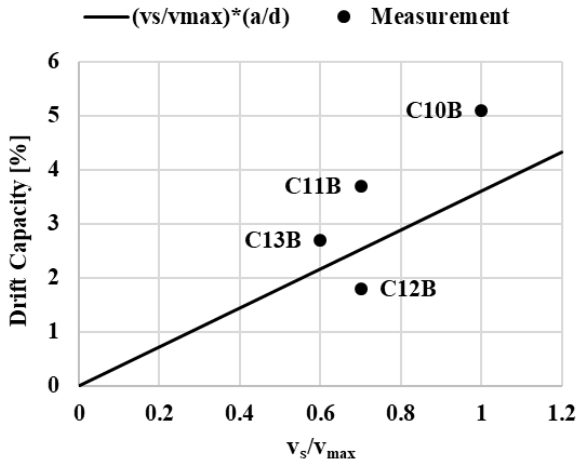

Figure 27: Measured drift capacities versus expected drift capacity for columns with conventional ties.

Figure 27 shows measured drift capacities for the four columns versus the expected drift capacity for a similar column with conventional ties, represented by the straight black line. This line is defined by Eq. 7, which was proposed by Ramirez et al. [35].

$$D.C. = \frac{r_{tr} \cdot f_y}{v_{max}} \quad (7)$$

where:

r = transverse reinforcement area ratio of conventional ties, calculated using Eq. 1;
f_y = yield stress of conventional ties;
v_{max} = maximum unit shear stress (Maximum shear force divided by the product $b * d$.

Unsuccessful repairs can be examined from two viewpoints:

- Analysis of the following ratios of shear strength to shear demand:
  - Nominal unit resistance to shear (v_n) to the maximum measured shear stress ($v_{\max}$).
  - Nominal contribution to shear of the transverse reinforcement (v_s) to the maximum measured shear stress ($v_{\max}$).

  Table 4 presents the ratios (v_n/v_{max} and v_s/v_{max}).
- Analysis of the lateral expansion of the concrete core (ε_{cc}). Table 5 presents estimates of Peak ($\varepsilon_{cc-peak}$) and Permanent ($\varepsilon_{cc-perm}$) core expansion for each column in Stages A, B, and C. Table 5 also includes estimates of core expansion after the application of post-tensioning in the clamps and estimates of core expansion associated with $0.8V_{max}$.

The following Sections titled: "*Analysis of nominal shear resistance vs shear demand*" and "*Analysis of concrete core lateral expansion*" present a discussion of the values listed in Tables 4 and 5.

Table 4: Nominal shear resistance and shear measured demands.

Column	Stage	v_s [MPa]	v_c [MPa]	v_n [MPa]	v_p [MPa]	v_n/v_p	V_{max} [kN]	v_{max} [MPa]	v_n/v_{max}	v_s/v_{max}	D.C. [%]
C10	A	0	1.4	1.4	2.3	0.6	550	2.6	-	0	5.1
	B	2.6		4		-			1.5	1	
C11	A	0.6		2		0.9	525	2.5	-	-	3.7
	B	1.8		3.2		-			1.3	0.7	
C12	A	0.6		2		0.9	410	1.9	-	-	1.8
	B	1.8		3.2		-			1.3*	0.7*	
C13	A	0.8		2.2		0.9	540	2.5	-	-	2.7
	B	1.5		2.9		-			1.2	0.6	
	C	1.5		2.9		-			1.2	0.6	

where:

v_s = nominal contribution to shear of the transverse reinforcement, including internal ties and external clamps;
v_{str} = nominal contribution to shear of the conventional ties;
v_{spt} = nominal contribution to shear of the post-tensioned clamps;
v_c = nominal contribution to shear of the concrete, estimated from the test of Column 10 in Stage A;
v_n = nominal unit resistance to shear (Eq. 4);
v_p = unit plastic shear stress (Eq. 5b);
V_{max} = maximum shear force measured in the test;
v_{max} = shear stress associated with V_{max}, calculated as $V_{max}/(b * d)$;
$D.C.$ = drift ratio associated with 20% decrease in the lateral load resistance of the column. It is calculated with help of an envelope of the load-displacement loops. Two values of drift capacities are obtained (pulling and pushing directions), but only the smaller value is reported.
*values calculated using v_{max} as the average of the maximum shear stress in the tests where flexural yielding occurred (C10, C11, and C13).

Table 5: Estimates of lateral concrete core expansion.

Column	Gauge Details		Stage A		Repair	Stage B		Repair	Stage C		ε_{cc} at $0.8V_{max}$ (Stage)
	Rel. length	Rel. position	$\varepsilon_{cc\text{-}peak}$	$\varepsilon_{cc\text{-}perm}$	ε_{cc} after P.T.	$\varepsilon_{cc\text{-}peak}$	$\varepsilon_{cc\text{-}perm}$	ε_{cc} after P.T.	$\varepsilon_{cc\text{-}peak}$	$\varepsilon_{cc\text{-}perm}$	
	L_o/b	h_g/h	[%]	[%]	[%]	[%]	[%]	[%]	[%]	[%]	[%]
C10	0.77	0.79	1.2	0.9	0.1	>8	N.A.	N.A.	N.A.	N.A.	2.9 (B)
C11	0.76	0.66	0.5	0.5	0.04	>7	N.A.	N.A.	N.A.	N.A.	2 (B)
C12	0.74	0.78	5.2	4.7	2.5	>8	N.A.	N.A.	N.A.	N.A.	2.8 (A)
C13	0.79	0.49	0.7	0.5	0.2	2.1	2	1.5	>7	N.A.	2.1 (B)

where: L_o = gauge length of the column concrete core. It is the distance between two particles located near the external faces of the outermost layers of longitudinal reinforcement;
b = width of the column;
h_g = vertical position at which cross-sectional strains of the concrete core were measured. Zero vertical position is at the top face of the foundation;
h = depth of the column;
$\varepsilon_{cc-peak}$ = peak concrete core expansion reached in each Stage;
$\varepsilon_{cc-perm}$ = permanent concrete core expansion at end of Stage. It is measured at zero lateral load.

Analysis of Nominal Shear Resistance vs Shear Demand

Figure 28 illustrates the nominal resistance to shear of the columns during each loading stage (A, B, and C). The plots show the shear resistance divided into three components:

- The contribution to shear of the concrete (v_c): It is assumed to be 1.4 MPa ($0.3\sqrt{f'_c}$), and it is estimated from the test of C10 in Stage A, as described in the Section *Column C10*.
- The contribution to shear of the transverse reinforcement (v_s): It is divided into two components: the contribution from conventional ties v_{str} and the contribution from the post-tensioned clamps v_{spt}. These two values are summed to obtain the total contribution to shear resistance of the transverse reinforcement v_s.
- The total nominal unit resistance to shear (v_n): It is calculated using Eq. 4, and it represents the combined shear resistance from both the concrete (v_c) and the transverse reinforcement (v_s).

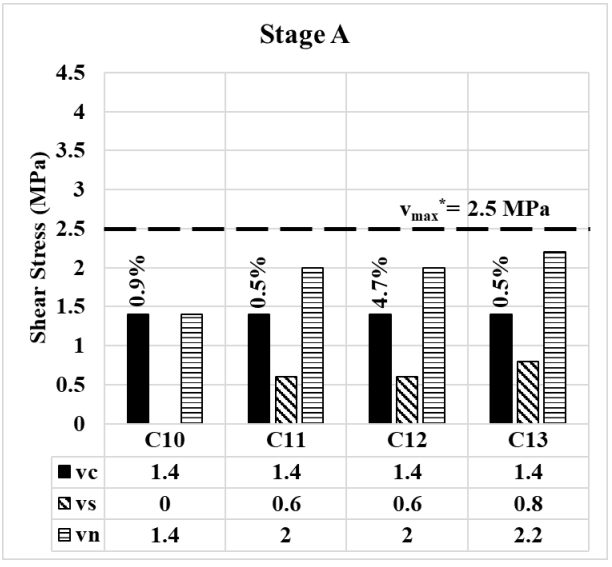

a) Stage A

Note: The percentage figures on top of the bars representing the concrete resistance to shear v_c correspond to the permanent core expansion ($\varepsilon_{cc-perm}$) at the end of the stage.

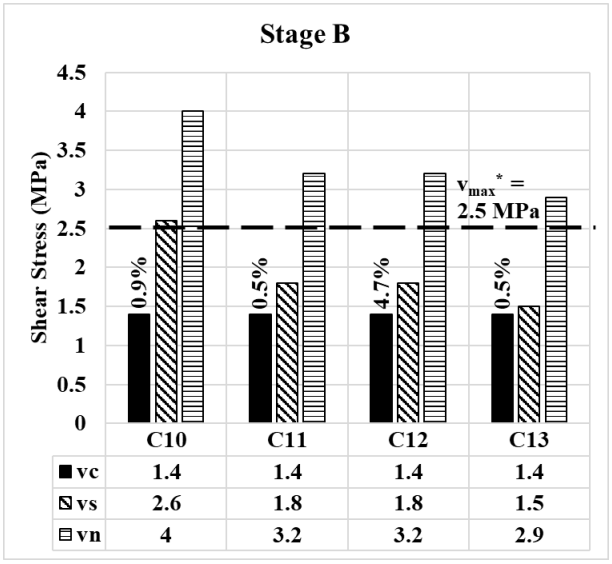

b) Stage B

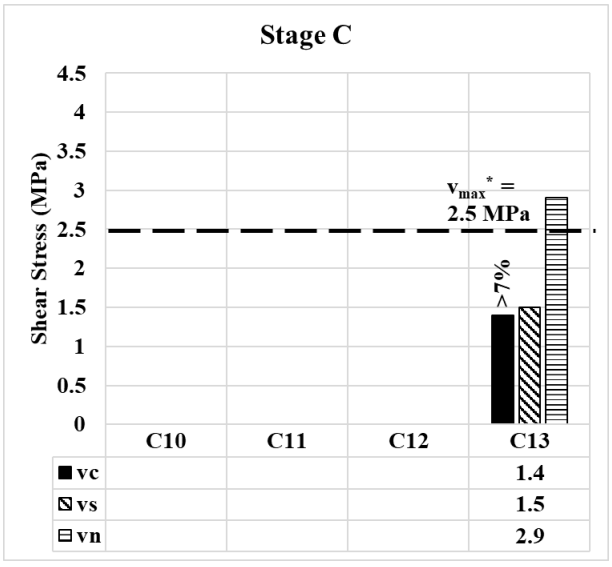

c) Stage C

Figure 28: Shear resistance – Stages A, B, and C.

The horizontal dashed line represents the average of the maximum measured shear stresses v_{max} in the tests of the columns that reached flexural yielding (C10, C11, and C13). The maximum shear stresses values are listed in Table 4, and the average is 2.5 MPa.

Figures 28b and 28c show that, in all cases, the nominal resistance to shear v_n exceeded the shear demand v_{max}=2.5 MPa after repairs. Table 4 lists the ratios v_n/v_{max}. Despite the ratio v_n/v_{max} being always larger than 1, there were still instances of unsuccessful repairs, such as C12 in Stage B, and C13 in Stage C. The nominal resistance to shear v_n includes a component attributed to the contribution to shear of the concrete v_c. This contribution has been assumed to decrease during loading reversals in the nonlinear range of response [36–38]. Damage of the columns before repairs may have led to a contribution to shear of the concrete smaller than 1.4 MPa ($0.3\sqrt{f'_c}$), which was the measured shear stress at the formation of critical inclined cracking in C10 during Stage A. Therefore, instead of v_n/v_{max}, it may be safer to consider the ratio v_s/v_{max} (Table 4) as an index to judge the efficiency of a repair. C10 in Stage B was the only column where the contribution to shear of the transverse reinforcement v_s exceeded the maximum shear demand v_{max}. Column C10 initially failed in shear at a drift ratio of 0.65%, and after providing clamps so that $v_s > v_{max}$, C10 reached flexural yielding and a drift capacity of 5.1%. Nonetheless, C11 and C13 also reached flexural yielding and their deformation capacities were improved by the repair with clamps in spite of having v_s/v_{max}<1.0. The ratios v_s/v_{max} and v_n/v_{max} may help to explain why the repair in C10 was successful but they are not conclusive for the remaining cases. Observations on the concrete core lateral expansion provide additional evidence.

Analysis of Concrete Core Lateral Expansion

In Figure 28, the percentage values on top of the bars representing the concrete resistance to shear v_c correspond to the permanent core expansion ($\varepsilon_{cc-perm}$) at the end of the stage. These values are measurements prior to the repair with post-tensioning (PT) clamps. Table 5 lists permanent core expansion values, as well as values of lateral expansion after P.T., and values of the peak concrete core expansion ($\varepsilon_{cc-peak}$). Cross-sectional strains (i.e. values of lateral expansion) of the concrete core were measured between two points located near the external faces of the outermost layers of longitudinal reinforcement as explained in the Section "*Concrete Core Lateral Expansion*". A relationship between concrete core expansion and applied drift ratio is presented in Figure 29 for each test column.

In Figure 29, the vertical dashed lines represent the drift ratios at which the repairs were conducted, while the vertical dotted lines indicate the drift ratios at which the lateral resistance of the column decreased by 20%. Note that for C13, two dashed lines are drawn because of the two repairs performed on this particular column.

The repairs conducted on C10, C11, and the first repair of C13 were successful (leading to yielding of longitudinal reinforcement and drift capacities exceeding 2%) despite the abruptness of the failure of C13 after its initial repair. These repairs were done after permanent concrete core expansions not exceeding 1%. In contrast, the repairs carried out on C12 and the second repair of C13 were ineffective. These repairs were done after permanent concrete core expansions of 4.7% (C12) and 2.1% (C13). Although the application of clamps reduced the core expansion by 50% (for C12) and 25% (for C13), the core expansion rapidly increased again during subsequent loading cycles. Within the limitations of data, it appears prudent to opt for repairs with post-tensioned clamps only if the permanent concrete core lateral expansion is smaller than 1%. Additional research can inform whether this limit can be relaxed if the investigated clamps are applied after epoxy injection of cracks.

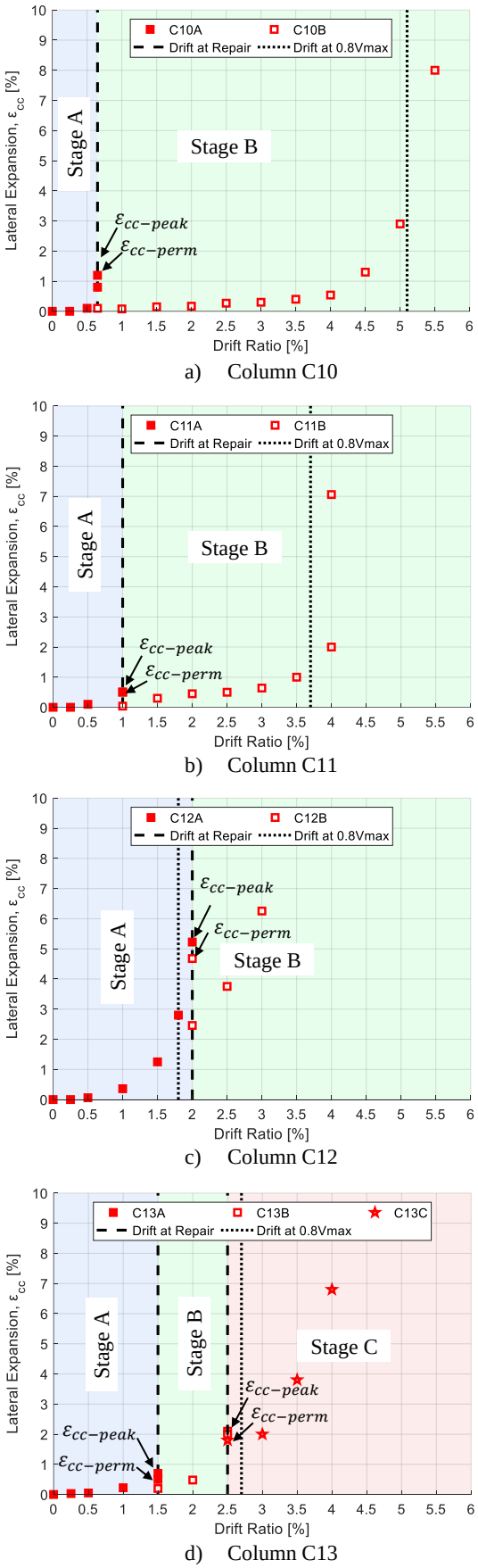

Figure 29: Lateral expansion ε_{cc} vs drift ratio.

Notice that C13, after repair, had the smallest ratio of v_s/v_{max} (0.6). And C10, in contrast, had the largest. Both were initially repaired after relatively small expansion (<1%), but the latter had a more ductile failure. It follows that it would be prudent to consider both a) expansion before repair, and b) the ratio v_s/v_{max}.

Measuring concrete expansion in the field is difficult. Nevertheless, a clear correlation between peak crack width and core expansion was observed (Figure 30). Peak crack width was determined as the largest crack thickness (width) measured at maximum drift applied before repair. Maximum shear crack and flexural crack widths are reported in Table 3. Figure 30 shows in the horizontal axis the ratio of peak crack width to gauge length. The gauge length is the distance between two particles located near the external faces of the outermost layers of longitudinal reinforcement. In the vertical axis, Figure 30a shows the peak cross-sectional expansion and Figure 30b shows the permanent cross-sectional expansion. The peak expansion is the maximum concrete core lateral expansion measured in the loading stage prior repair. The permanent expansion is the maximum concrete core lateral expansion measured with NO lateral load applied in the column and prior repair. The round black markers represent measurements at the end of Stage A for C10, C11, and C12, and at the end of Stages A and B for C13. The dashed line is the line of best fit to the data points, calculated as a linear regression with intercept in the origin (0,0).

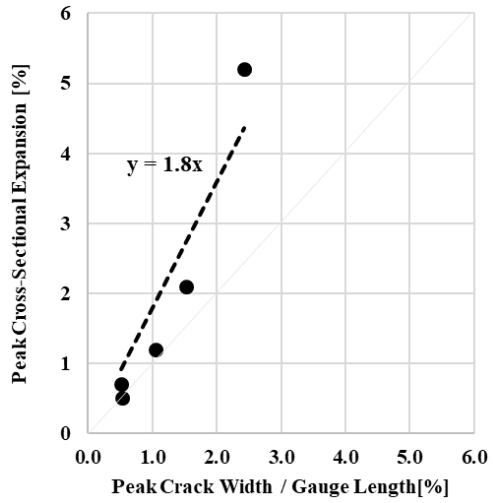

a)

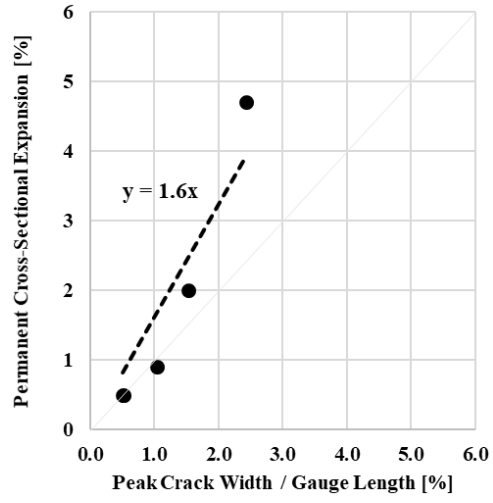

b)

Figure 30: Peak crack width vs peak and permanent cross-sectional expansion.

Comparing Figures 30a and 30b suggests that peak lateral expansion, on average, is (1.8/1.6 – 1) ≈ 13% larger than permanent lateral expansion. Therefore, a ratio β of permanent crack width to distance between outer bars of 0.5% is inferred to correspond to a ratio of peak crack width to distance between outer bars of nearly 0.6% (to use a single significant figure in light of the scatter in Figure 30). Figure 30b suggests that the corresponding permanent cross-sectional expansion is 1.6x0.6 ≈ 1%. In absence of a better way to estimate core expansion in the field and given the preceding discussion, it is therefore suggested to avoid using clamps as the sole repair method for columns with $\beta > 0.5\%$. It is recommended that the ability of other repair methods (e.g. steel and FRP jackets) to restore the integrity of a damaged RC column also be evaluated in columns with different degrees of initial damage quantified in terms of core expansion or other more significant terms, if any.

Another salient observation is the correlation between core expansion and drift at which lateral resistance had decreased by at least 20% of the maximum shear ($0.8V_{max}$). Table 5 presents the values of core expansion associated with $0.8V_{max}$, and the stage in which it occurred in parentheses. At the mentioned drift, the core expansion was observed to range from 2 to 3% (2.9, 2, 2.8, and 2.1 for C10, C11, C12, and C13, respectively) This observation is in agreement with observations by Ramirez et al. [39] who reported lateral expansions of approximately 3% during cycles associated with the mentioned decrease in lateral resistance of 20%. Figure 31 shows the values of core expansion associated with $0.8V_{max}$ for both test columns in this study and the P1-P6 columns tested by Ramirez et al. [39].

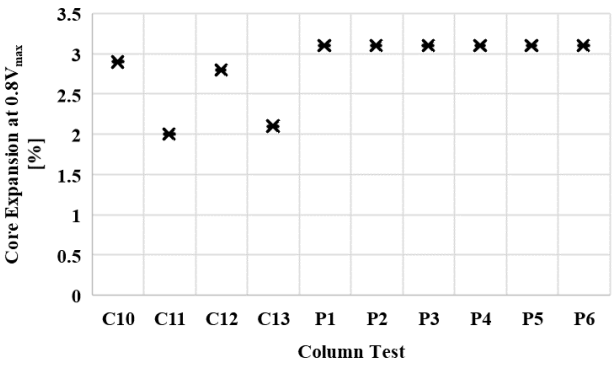

Figure 31: Concrete core expansion at $0.8V_{max}$.

CONCLUSIONS

Within the ranges of the parameters and variables listed in Tables 1 and 2, the following observations were made:

1. Repair with post-tensioned clamps was observed to be successful when the maximum permanent cross-sectional lateral expansion (at zero lateral load) measured before repair was smaller than 1%.
2. Columns repaired with clamps before the permanent cross-sectional expansion exceeded 1% were observed to reach their expected flexural strengths during testing done after repair in cases in which $0.6<v_s/v_{max}<1$. Nonetheless, given how hard it is to estimate the contribution to shear from the concrete, v_c, it is recommended to design repairs ignoring v_c and providing enough clamps to that $v_s/v_{max} \geq 1$. The combination of $v_s/v_{max} \geq 1$ and core expansions at repair $< 1\%$ led to the best results.

   where: v_s = nominal contribution to shear of the transverse reinforcement, including internal ties and external clamps;
   v_c = nominal contribution to shear of the concrete;
   v_{max} = shear stress associated with V_{max}, calculated as $V_{max}/(b*d)$;
   V_{max} = maximum shear force measured in the test;
   b = width of the column; and

d = effective depth: distance from extreme layer of bars in tension to extreme layer of concrete in compression.

3. The peak cross-sectional expansion was observed to be nearly 2 times the ratio of permanent crack width to distance between outer layers of bars, β. It is suggested to avoid using clamps as the sole repair method for columns with β >0.5%.
4. It is recommended that the ability of other repair methods (e.g. steel and FRP jackets) to restore the integrity of a damaged RC column also be evaluated in columns with different degrees of initial damage. Limits to how much damage can be repaired with given repair techniques are needed.
5. The lateral expansion of the concrete core at $0.8V_{max}$ ranged between 2% and 3%. $0.8V_{max}$ corresponds to the shear force associated with the drift capacity (as defined in Table 3).

ACKNOWLEDGMENTS

This project was supported by QuakeCoRE (New Zealand Centre for Earthquake Resilience) and the University of Canterbury in the form of physical and human resources. Many thanks to the Resilience to Nature's Challenges Project for the 3-years postgraduate scholarship awarded.

The main author is thankful to the New Zealand Society for Earthquake Engineering (NZSEE) for the 2022 Research Scholarship Award.

Special thanks to the Structures Laboratory staff for their support during the experimental work, and to Professor Roger Nokes and Dr. Justin Brown for their guidance on how to use the software Streams.

REFERENCES

1 DeBlasio AJ, Zamora A, Mottley F, Brodesky R, Zirker ME, Crowder M and John A (2002). "*Effects of Catastrophic Events on Transportation System Management and Operations: Northridge Earthquake, January 17, 1994. United States*". Volpe National Transportation Systems Center, Joint Program Office for Intelligent Transportation Systems, USA. https://rosap.ntl.bts.gov/view/dot/39118

2 Decanini LD, De Sortis A, Goretti A, Liberatore L, Mollaioli F and Bazzurro P (2004). "Performance of reinforced concrete buildings during the 2002 Molise, Italy, earthquake". *Earthquake Spectra*, **20**: 221–255. https://doi.org/10.1193/1.1765107

3 Bayraktar A, Altunişik AC and Pehlivan M (2013). "Performance and damages of reinforced concrete buildings during the October 23 and November 9, 2011 Van, Turkey, earthquakes". *Soil Dynamics and Earthquake Engineering*, **53**: 49–72. https://doi.org/10.1016/j.soildyn.2013.06.004

4 Baran E, Mertol HC and Gunes B (2014). "Damage in reinforced concrete buildings during the 2011 Van, Turkey, earthquakes". *Journal of Performance of Constructed Facilities*, American Society of Civil Engineers (ASCE), **28**: 466–479. https://doi.org/10.1061/(ASCE)CF.1943-5509.0000396

5 Vandoros KG and Dritsos SE (2008). "Concrete jacket construction detail effectiveness when strengthening RC columns". *Construction and Building Materials*, **22**: 264–276. https://doi.org/10.1016/j.conbuildmat.2006.08.019

6 Lehman DE, Gookin SE, Nacamuli AM and Moehle JP (2001). "Repair of earthquake-damaged bridge columns". *ACI Structural Journal*, American Concrete Institute, **98**: 233–242. https://doi.org/10.14359/10192

7 Priestley MJN, Seible F, Xiao Y, et al. (1994). "Steel jacket retrofitting of reinforced concrete bridge columns for enhanced shear strength - Part 2: Test results and comparison with theory". *Structural Journal*, **91**: 537–551. https://www.concrete.org/publications/internationalconcreteabstractsportal/m/details/id/4168

8 Aboutaha RS, Engelhardt MD, Jirsa JO and Kreger ME (1999). "Rehabilitation of shear critical concrete columns by use of rectangular steel jackets". *ACI Structural Journal*, American Concrete Institute, **96**: 68–78. https://doi.org/10.14359/597

9 Fakharifar M, Chen G, Sneed L and Dalvand A (2015). "Seismic performance of post-mainshock FRP/steel repaired RC bridge columns subjected to aftershocks". *Composites Part B Engineering*, **72**: 183–198. https://doi.org/10.1016/j.compositesb.2014.12.010

10 Fakharifar M, Chen G, Wu C, Shamsabadi A, ElGawady MA and Dalvand A (2016). "Rapid repair of earthquake-damaged RC columns with prestressed steel jackets". *Journal of Bridge Engineering*, American Society of Civil Engineers (ASCE), **21**: 04015075. https://doi.org/10.1061/(asce)be.1943-5592.0000840

11 Chang S-Y, Li Y-F and Loh C-H (2004). "Experimental study of seismic behaviors of as-built and carbon fiber reinforced plastics repaired reinforced concrete bridge columns". *Journal of Bridge Engineering*, American Society of Civil Engineers (ASCE), **9**: 391–402. https://doi.org/10.1061/(ASCE)1084-0702(2004)9:4(391)

12 Rutledge ST, Kowalsky MJ, Seracino R and Nau JM (2014). "Repair of reinforced concrete bridge columns containing buckled and fractured reinforcement by plastic hinge relocation". *Journal of Bridge Engineering*, American Society of Civil Engineers (ASCE), **19**: A4013001. https://doi.org/10.1061/(ASCE)BE.1943-5592.0000492

13 Yang Y, Sneed L, Saiidi MS, Belarbi A, Ehsani M and He R (2015). "Emergency repair of an RC bridge column with fractured bars using externally bonded prefabricated thin CFRP laminates and CFRP strips". *Composite Structures*, **133**: 727–738. https://doi.org/10.1016/j.compstruct.2015.07.045

14 Bouchelaghem H, Bezazi A and Scarpa F (2011). "Compressive behaviour of concrete cylindrical FRP-confined columns subjected to a new sequential loading technique". *Composites Part B Engineering*, **42**: 1987–1993. https://doi.org/10.1016/j.compositesb.2011.05.045

15 Ispir M, Dalgic KD and Ilki A (2018). "Hybrid confinement of concrete through use of low and high rupture strain FRP". *Composites Part B Engineering*, **153**: 243–255. https://doi.org/10.1016/j.compositesb.2018.07.026

16 Wahab S and Hussain C (2019). "Performance of concrete confined with a jute–polyester hybrid fiber reinforced polymer composite: A novel strengthening technique". *Fibers (Basel, Switzerland)*, MDPI AG, **7**: 72. https://doi.org/10.3390/fib7080072

17 Ishibashi T, Tsuyoshi T and Kobayashi K (2004). "Seismic retrofitting methods newly developed for railway concrete structures". *Journal of Advanced Concrete Technology*, **2**: 65–76. https://doi.org/10.3151/jact.2.65

18 Reddit. *External Reinforcement in Shinkansen RC Columns near Fukuyama Station in Japan*. https://www.reddit.com/r/InfrastructurePorn/comments/b52j1e/external_reinforcement_of_concrete_pillars_for/

19 Lunoe RR and Willis A (1957). "Application of steel strap reinforcement to girders of rigid frames, special AMC warehouses". *Journal Proceedings*. https://www.concrete.org/publications/internationalconcreteabstractsportal/m/details/id/11541

20 Yamakawa T, Kooroush NN and Satoh H (2001). "Seismic or emergency retrofit of RC short columns by use of prestressed Aramid fiber belts as external hoops". *Journal of Structural and Construction Engineering*, Architectural Institute of Japan, **66**: 135–141. https://www.jstage.jst.go.jp/article/aijs/66/550/66_KJ00004101651/_article/-char/ja/

21 Miyagi T, Yamakawa T, Li W and Rahman M (2004). "A study on emergency retrofit using prestressing bars and steel plates for damaged columns". *Proceedings of Thirteenth World Conference on Earthquake Engineering*. http://www.iitk.ac.in/nicee/wcee/article/13_1169.pdf

22 Kyoda N, Yamakawa T, Nakada K, Javadi P and Nagahama A (2011). "Emergency retrofit for damaged RC columns by fiber belts prestressing and plywoods". *Advances in FRP Composites in Civil Engineering*, 801–805. https://doi.org/10.1007/978-3-642-17487-2_176

23 Jung D, Wilcoski J and Andrawes B (2018). "Bidirectional shake table testing of RC columns retrofitted and repaired with shape memory alloy spirals". *Engineering Structures*, **160**: 171–185. https://doi.org/10.1016/j.engstruct.2017.12.046

24 Lagoudas DC. *Shape Memory Alloys*. Springer US. https://doi.org/10.1007/978-0-387-47685-8

25 Yamakawa T, Kamogawa S and Kurashige M (2000). "Seismic performance and design of RC columns retrofitted by PC bar prestressing as external hoops". *Journal of Structural and Construction Engineering, AIJ*, **537**: 107–113. https://ci.nii.ac.jp/naid/10018682035/

26 Skillen KC (2020). "T*he Effects of Transverse Reinforcement on the Strength and Deformability of RC Elements*". PhD Dissertation, University of Purdue. https://hammer.figshare.com/articles/thesis/The_Effects_of_Transverse_Reinforcement_on_the_Strength_and_Deformability_of_Reinforced_Concrete_Elements/13377242

27 Rincon JD, Skillen KC, Pujol S, Chen Y-M, Puranam AY and Hwang AS-J (2023). "Active confinement of RC columns with external post-tensioned clamps". *ACI Symposium Publication*, **358**. https://doi.org/10.14359/51740233

28 Rincon JD, Chen YM, Pujol S, Puranam AY and Hwang SJ (2024). "Shear strength of reinforced concrete columns with external post-tensioned clamps". *ACI Structural Journal*, American Concrete Institute, **121**. https://doi.org/10.14359/51740248

29 Rincon JD, Chen YM, Pujol S, Puranam AY, Hwang SJ and Hibino Y (2024). "Drift capacity of RC columns strengthened with post-tensioned external clamps. *ACI Structural Journal*, **(In Review)**.

30 Richart FE (1927). *An Investigation of Web Stresses in Reinforced Concrete Beams*. University of Illinois.

31 Hognestad E (1951). "Study of combined bending and axial load in reinforced concrete members". *Bulletin of Illinois Engineering Experiment Station.* ideals.illinois.edu. https://www.ideals.illinois.edu/items/4902/bitstreams/19186/object

32 Nokes R (2020). *Streams Version 3.03 - System Theory and Design*.

33 Ottenhaus L-M, Li M, Nokes R, Cammock P and McInnes B (2019). "Use of particle tracking velocimetry in timber material and connection testing". *European Journal of Wood and Wood Products*, **77**: 195–209. https://doi.org/10.1007/s00107-018-1376-y

34 Brown J, Li M, Nokes R, Palermo A, Pampanin S and Sarti F (2020). "Investigating the compressive toe of post-tensioned CLT core-walls using particle tracking technology". *17th World Conference on Earthquake Engineering (17WCEE)*, Sendai, Japan.

35 Ramirez JA, Pujol S and Sozen MA (1999). "Drift capacity of reinforced concrete columns subjected to cyclic shear reversals". *Special Publication* **187**: 255–274. ftp://jetty.ecn.purdue.edu/spujol/CE571/Drift%20Capacity%20Summary%20and%20References/1.%20Column%20Drift%20Capacity%20-%20sp187-12%20[RAMIREZ].pdf

36 Brown RH and Jirsa JO (1971). "Reinforced concrete beams under load reversals". *Journal Proceedings*. https://www.concrete.org/publications/internationalconcreteabstractsportal.aspx?m=details&i=11338&m=details&i=11338

37 Wight JK and Sozen MA (1973). "*Shear strength decay in reinforced concrete columns subjected to large deflection reversals*". University of Illinois. Engineering Experiment Station. http://www.ideals.illinois.edu/bitstream/handle/2142/13817/SRS-403.pdf?sequence=2

38 Popov EP, Bertero VV and Krawinkler H (1972). "C*yclic behavior of three reinforced concrete flexural members with high shear*". Earthquake Engineering Research Center, College of Engineering, University of California. https://play.google.com/store/books/details?id=keSiAQAACAAJ

39 Pujol S, Sozen M and Ramirez J (2006). "Displacement history effects on drift capacity of reinforced concrete columns". *ACI Structural Journal*, American Concrete Institute, **103**. https://doi.org/10.14359/15183